Electronic Supplementary Material (ESI) for Nanoscale.

Supporting information for

Electrospun Hetero-CoP/FeP Embedded in Porous Carbon Nanofibers: Enhanced Na^+ Kinetics and Specific Capacity

Liang Han[a], Mutian Zhang[a], Huanlei Wang[a,*], Ping Li[a], Wenrui Wei[a], Jing Shi[a], Minghua Huang[a], Zhicheng Shi[a], Wei Liu[a] and Shougang Chen[a,*]

[a] *School of Materials Science and Engineering, Ocean University of China, Qingdao, 266100, People's Republic of China.*

E-mail: huanleiwang@gmail.com (H. Wang); sgchen@ouc.edu.cn (S. Chen)

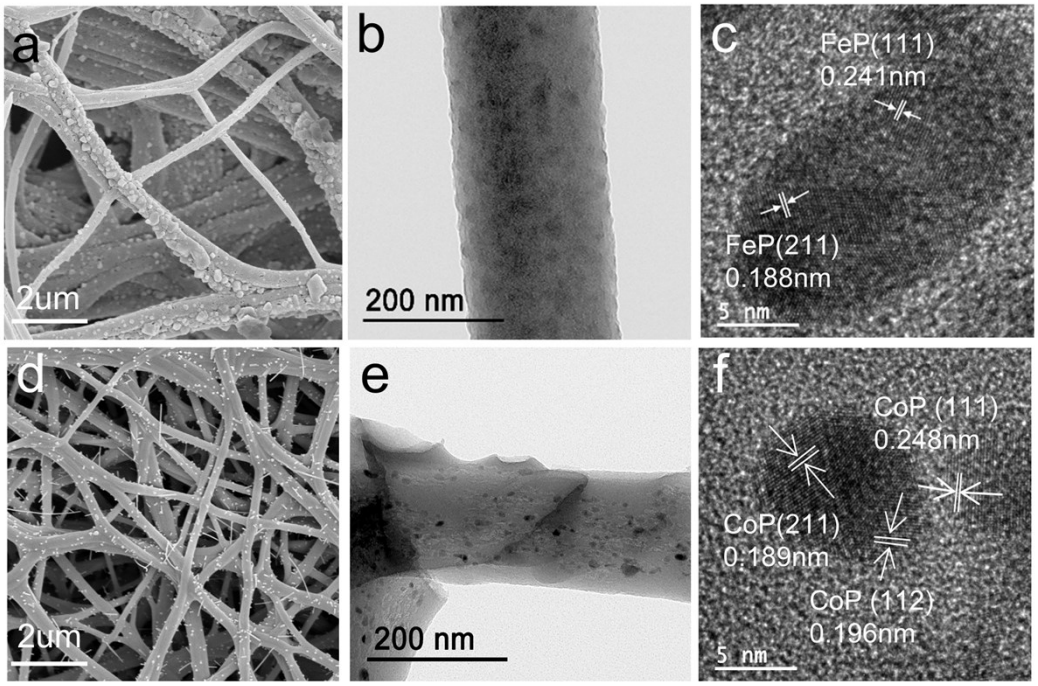

Fig. S1 (a) SEM and (b, c) TEM images of FeP@PCNFs. (d) SEM and (e, f) TEM images of CoP@PCNFs.

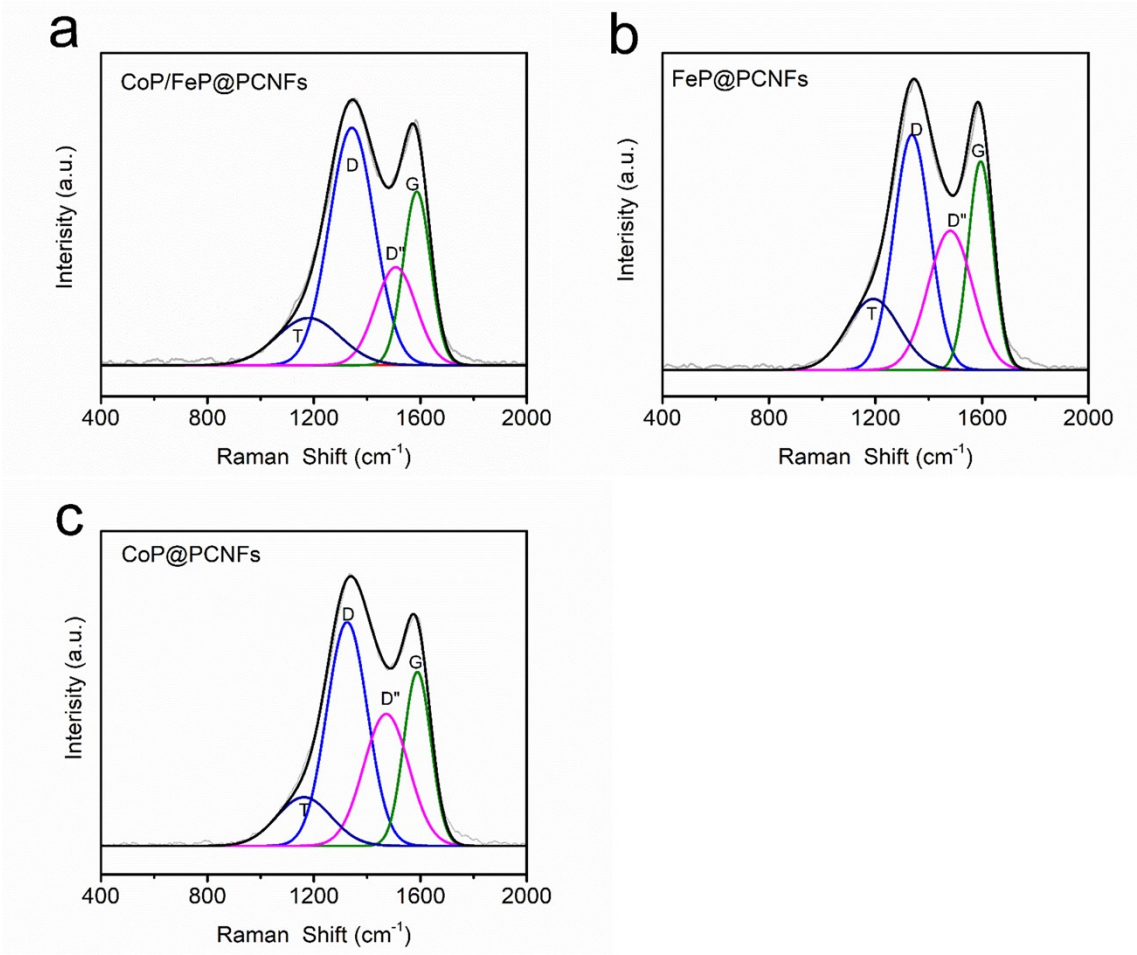

Fig. S2 Fitted Raman spectra of (a) CoP/FeP@PCNFs, (b) FeP@PCNFs, and (c) CoP@PCNFs electrodes.

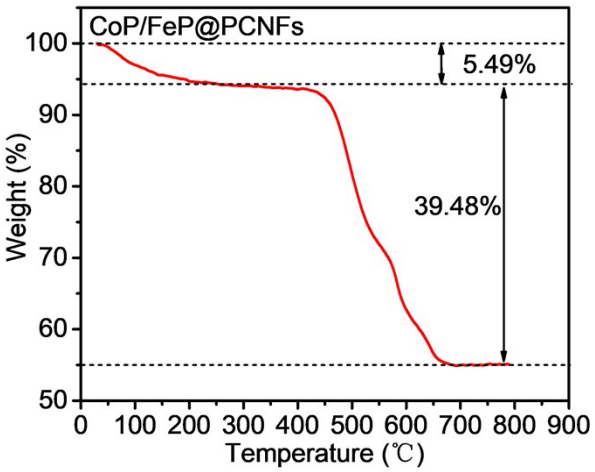

Fig. S3 TG curve of the CoP/FeP@PCNFs.

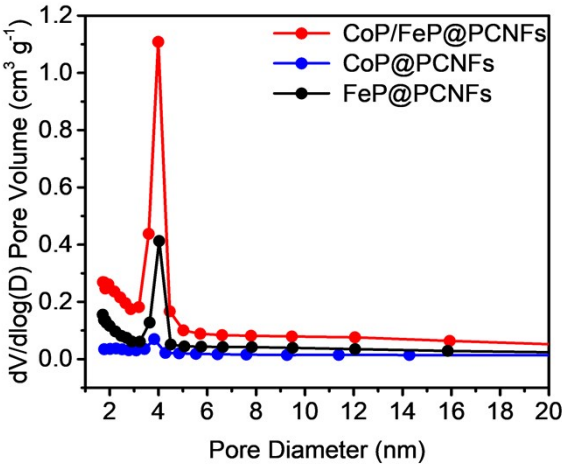

Fig. S4 BJH pore size distribution of CoP/FeP@PCNFs, CoP@PCNFs and FeP@PCNFs.

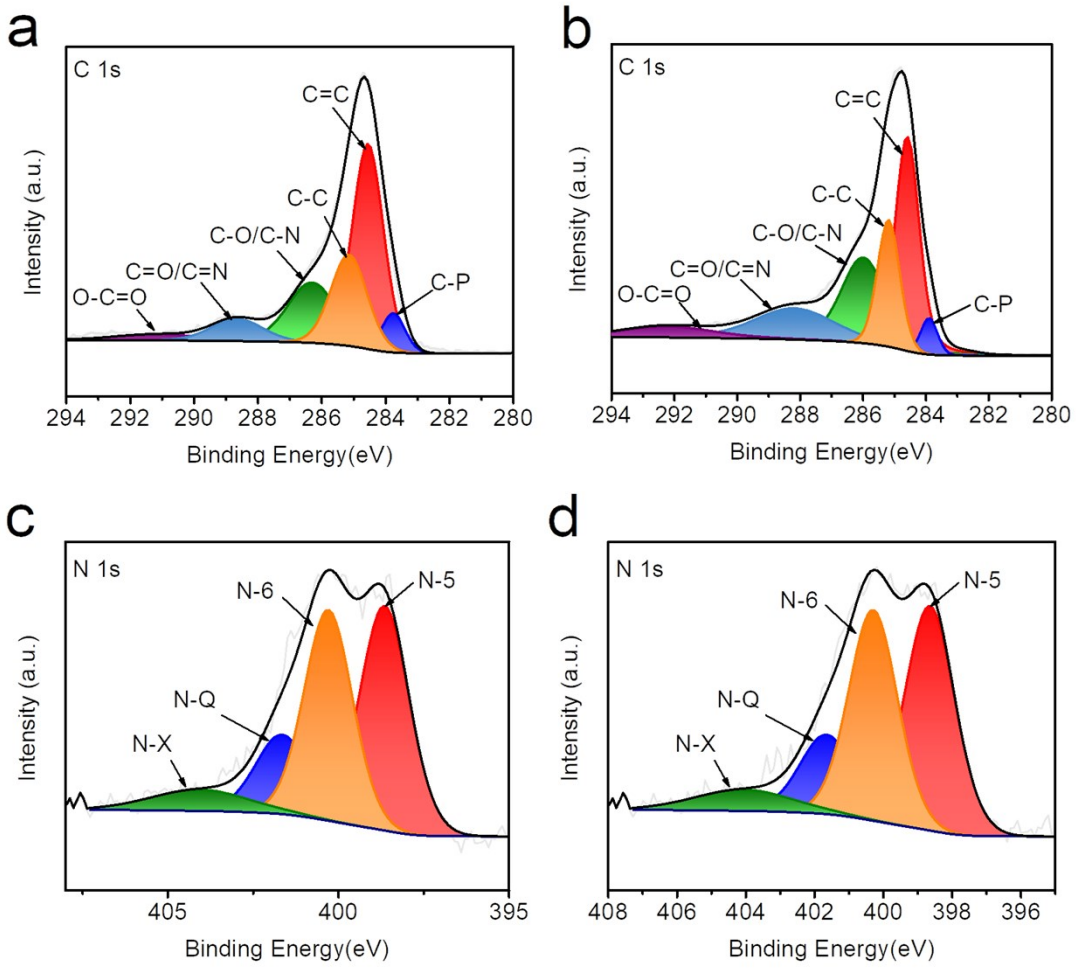

Fig. S5 High-resolution C1s XPS spectra of (a) CoP@PCNFs and (b) FeP@PCNFs. High-resolution N1s XPS spectra of (c) CoP@PCNFs and (d) FeP@PCNFs.

Table S1 Relative surface concentrations of nitrogen species in the three samples.

Sample	Relative peak areas (%)			
	N-Q	N-X	N-5	N-6
CoP/FeP@PCNFs	15.3	7.5	40.2	37.0
CoP@PCNFs	15.6	7.6	39.5	37.3
FeP@PCNFs	15.0	8.0	40.6	36.4

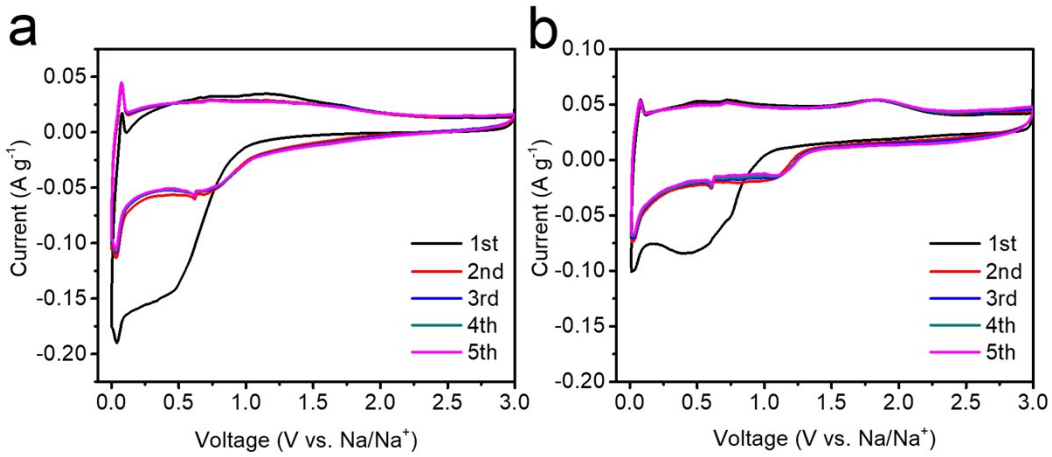

Fig. S6 CV curves of the (a) CoP@PCNFs and (b) FeP@PCNFs electrodes at 0.1 mV s^{-1}.

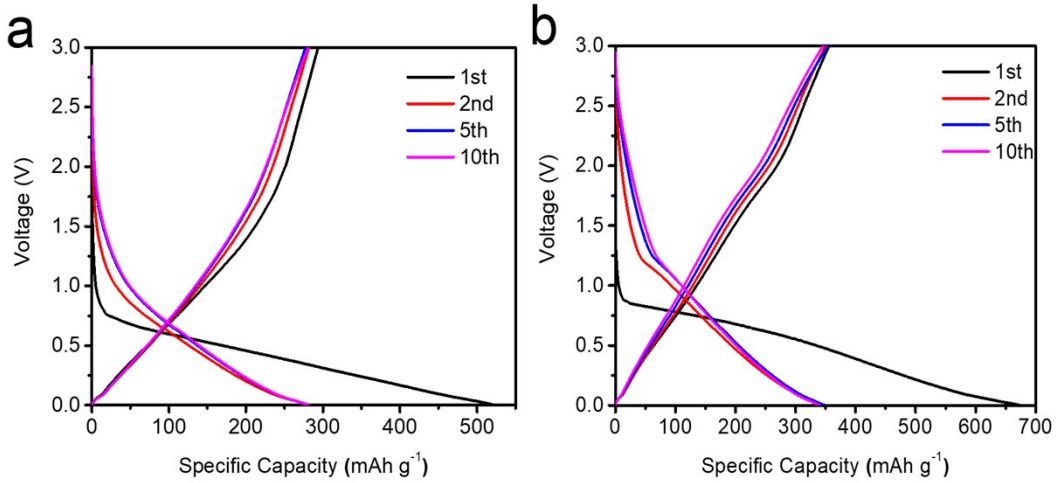

Fig. S7 The typical galvanostatic discharge/charge curves of the (a)CoP@PCNFs and (b) FeP@PCNFs electrode at the current density of 0.05 A g^{-1}.

Table S2. Comparison of sodium storage performance for the CoP/FeP@PCNFs with other metal phosphide-based electrodes.

Materials	Electrolyte	Rate capacity	Cycling stability	Ref.
CoP_3@C	1 M $NaClO_4$ in EC/DEC+5%FEC	344.1 mAh g^{-1} at 0.05A g^{-1} 136.4 mAh g^{-1} at 2.5 A g^{-1}	144 mAh g^{-1} after 260 cycles at 0.3A g^{-1}	1
Co_2P@N-C@rGO	1M $NaClO_4$ in EC/DEC	323 mAh g^{-1} at 0.05A g^{-1} 200 mAh g^{-1} at 0.5 A g^{-1}	225 mAh g^{-1} after 100 cycles at 0.05 A g^{-1}	2
CoP	1M $NaClO_4$ in PC+5%FEC	310 mAh g^{-1} at 0.1A g^{-1} 80 mAh g^{-1} at 2 A g^{-1}	315 mAh g^{-1} after 25 cycles at 0.1 A g^{-1}	3
MoP	1M $NaClO_4$ in PC+5%FEC	387 mAh g^{-1} at 0.1A g^{-1} 115 mAh g^{-1} at 1.6 A g^{-1}	104.5 mAh g^{-1} after 10000 cycles at 1.6 A g^{-1}	4
CNT@FeP-C	1M $NaClO_4$ in EC/PC	391 mAh g^{-1} at 0.2A g^{-1} 258 mAh g^{-1} at 5 A g^{-1}	295 mAh g^{-1} after 500 cycles at 0.5 A g^{-1}	5
FeP/graphite	1M $NaClO_4$ in EC/DEC	280 mAh g^{-1} at 0.05A g^{-1} 56 mAh g^{-1} at 2.5 A g^{-1}	175 mAh g^{-1} after 70 cycles at 0.05 A g^{-1}	6
FeP	1M $NaClO_4$ in PC+5%FEC	420 mAh g^{-1} at 0.05A g^{-1} 60 mAh g^{-1} at 0.5 A g^{-1}	321 mAh g^{-1} after 60 cycles at 0.05 A g^{-1}	7
CoP@C-RGO-NF	1.0 M $NaClO_4$ in PC =100 vol% with 5.0% FEC	543 mAh g^{-1} at 0.2A g^{-1} 155 mAh g^{-1} at 1.6 A g^{-1}	470 mAh g^{-1} after 100 cycles at 0.1 A g^{-1}	8
Cu_3P nanowire (CPNW)	1M $NaClO_4$ in EC/DEC+5%FEC	362 mAh g^{-1} at 0.1A g^{-1} 137 mAh g^{-1} at 5 A g^{-1}	349 mAh g^{-1} after 260 cycles at 1 A g^{-1}	9
MoP@C	1.0 M $NaCF_3SO_3$ in DEGDME	358 mAh g^{-1} at 0.05A g^{-1} 173 mAh g^{-1} at	180 mAh g^{-1} after 250 cycles at 0.5 A g^{-1}	10

		1 A g^{-1}		
NCP@FCNT-FS	1 M $NaClO_4$ in PC + 5 wt% FEC	401 mAh g^{-1} at 0.4A g^{-1} 276 mAh g^{-1} at 3.2 A g^{-1}	188.9 mAh g^{-1} after 100 cycles at 0.4 A g^{-1}	11
RGO@CoP@FeP	1 M $NaClO_4$ in PC +5 wt% FEC	480 mAh g^{-1} at 0.1A g^{-1} 374 mAh g^{-1} at 1A g^{-1}	456.2 mAh g^{-1} after 200 cycles at 0.1 A g^{-1}	12
NiCoP-NC	1.0 M $NaClO_4$ in EC/DEC	406.2 mAh g^{-1} at 0.1A g^{-1} 202.1 mAh g^{-1} at 3A g^{-1}	334.8 mAh g^{-1} after 200 cycles at 0.1 A g^{-1}	13
Ti_3C_2/NiCoP	1 M $NaClO_4$ in EC:DMC:EMC + 5 wt% FEC	416.9 mAh g^{-1} at 0.1A g^{-1} 240 mAh g^{-1} at 2A g^{-1}	261.7 mAh g^{-1} after 2000 cycles at 1 A g^{-1}	14
This work	1M $NaSO_3CF_3$ in DGM	459 mAh g^{-1} at 0.05A g^{-1} 213 mAh g^{-1} at 10 A g^{-1}	208 mAh g^{-1} after 1000 cycles at 5 A g^{-1}	

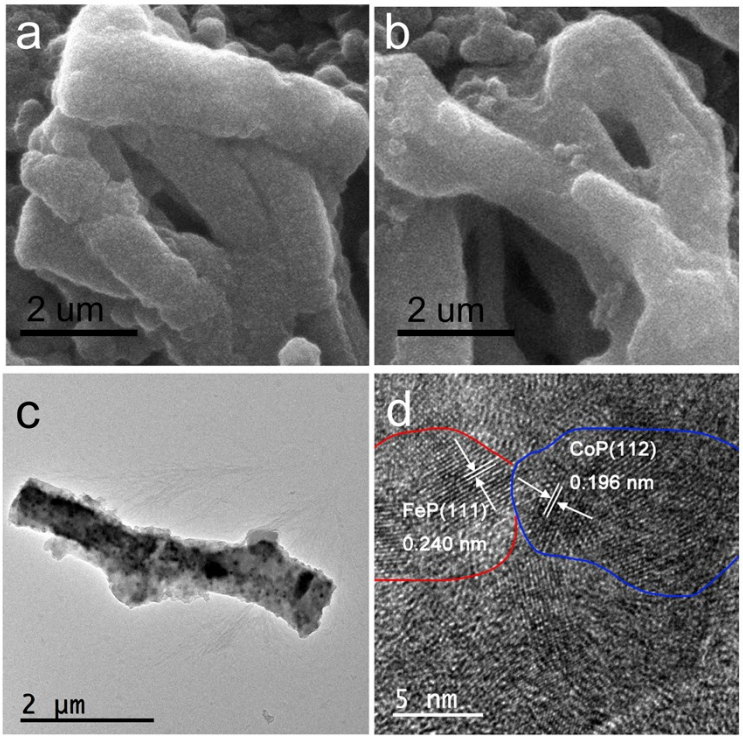

Fig. S8 (a,b) SEM and (c,d) TEM images of CoP/FeP@PCNFs after 1000 cycles.

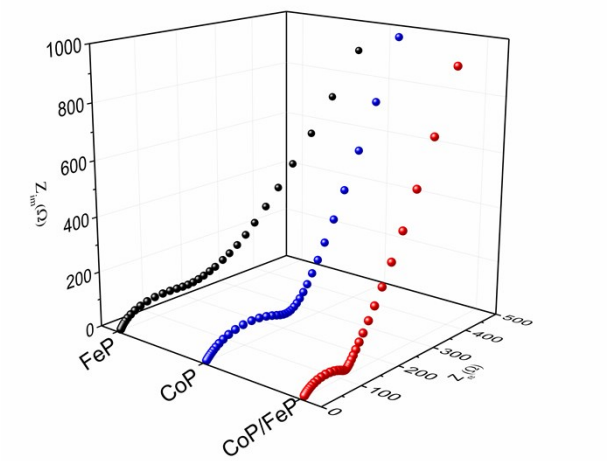

Fig. S9 EIS spectra of CoP/FeP@PCNFs, CoP@PCNFs and FeP@PCNFs electrodes before cycling.

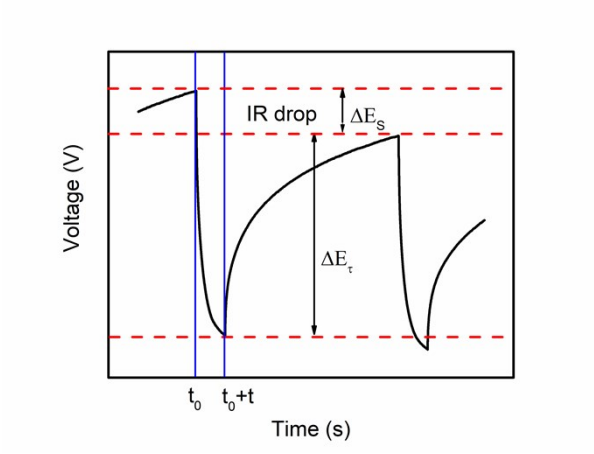

Fig.S10 Schematic for the calculation method employed. The analysis was based on an applied current of 22 mA g^{-1} for 0.5 h, followed by a 3 h relaxation.

GITT tests were performed to characterize sodium-ion diffusion coefficient (D_{Na}) in the synthesized samples. The GITT data of CoP/FeP@PCNFs, CoP@CNFs and FeP@PCNFs were recorded at a constant current density of 22 mA g^{-1} for an interval of 30 min followed by 180 min relaxation in the first cycle. D_{Na} value of CoP/FeP@PCNFs electrodes is based on the following Equation:

$$D_{Na^+} = \frac{4}{\pi\tau}\left(\frac{m_B V_m}{M_b S}\right)^2 \left(\frac{\Delta E_s}{\Delta E_\tau}\right)^2$$

where τ denotes the constant current pulse time, m_B, V_m, and M_b are the mass, molar volume, molar mass of the material, S is the area of electrode-electrolyte interface. ΔE_s refers to voltage change during a single-step experiment, and ΔE_τ is the total change of cell voltage during a constant current pulse.

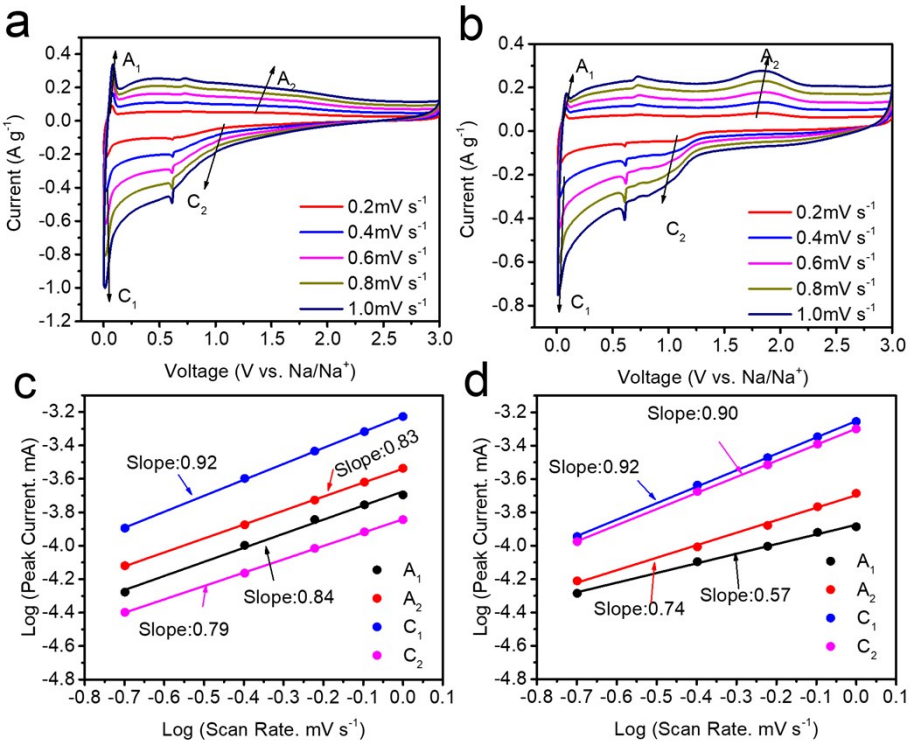

Fig. S11 CV curves of (a) CoP@PCNFs and (b) FeP@PCNFs electrode at different scan rates. Cathodic and anodic b values of (c) CoP@PCNFs, (d) FeP@PCNFs.

The CASTEP software package requires that the calculation system must be periodic, and the calculation requires that the structure should have a large enough vacuum layer to accurately determine the energy level at the vacuum and eliminate the influence of interlayer interaction[15]. Therefore, a vacuum layer is added to make the total length of Z direction 25 Å to establish periodic cells. BFGS optimization algorithm was used for geometric optimization. The heterogenous crystal lattice distortion was less than 5% and 2.28%, which is far less than the general requirements for the construction of heterogeneous lattice distortion. The interval between the layers is 3.019 Å, which is close to that of the general two-dimensional van der Waals heterogeneous junction. Therefore, it can be considered that the model constructed by us is reasonable.

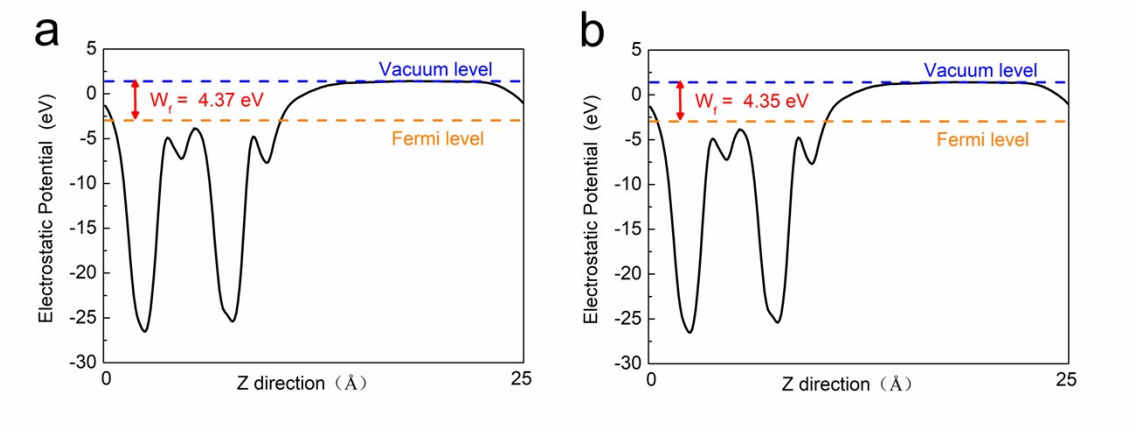

Fig. S12 Electrostatic potential drop diagram of (a) FeP homogeneous junction and (b)CoP homogeneous junction.

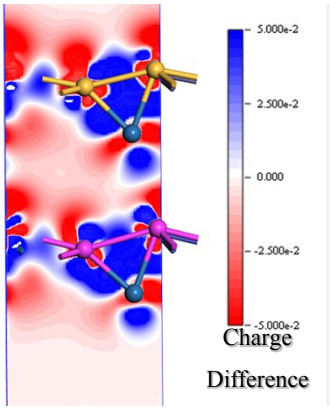

Fig. S13 Side view of an interlayer differential charge density diagram for a CoP/FeP heterostructure.

Table. S3 Mean Mulliken charge density of Fe, Co, P atoms in CoP/FeP heterostructure, FeP

homogeneous junction and CoP homogeneous junction.

System/atom	Fe	Co	P
FeP	0.115	/	-0.115
CoP	/	0.221	-0.221
FeP/CoP	0.143	0.266	-0.125

Notes and references

1. W. Zhao, X. Ma, G. Wang, X. Long, Y. Li, W. Zhang and P. Zhang, *Appl. Surf. Sci.*, 2018, **445**, 167-174.
2. R. Jin, X. Li, Y. Sun, H. Shan, L. Fan, D. Li and X. Sun, *ACS Appl. Mater. Interfaces*, 2018, **10**, 14641-14648.
3. W.-J. Li, Q.-R. Yang, S.-L. Chou, J.-Z. Wang and H.-K. Liu, *J. Power Sources*, 2015, **294**, 627-632.
4. Z. Huang, H. Hou, C. Wang, S. Li, Y. Zhang and X. Ji, *Chem. Mater.*, 2017, **29**, 7313-7322.
5. F. Han, C. Y. J. Tan and Z. Gao, *Chem. Electro. Chem.*, 2016, **3**, 1054-1062.
6. Q.-R. Yang, W.-J. Li, S.-L. Chou, J.-Z. Wang and H.-K. Liu, *RSC Adv.*, 2015, **5**, 80536-80541.
7. W. J. Li, S. L. Chou, J. Z. Wang, H. K. Liu and S. X. Dou, *Chem. Commun.*, 2015, **51**, 3682-3685.
8. X. Ge, Z. Li and L. Yin, *Nano Energy*, 2017, **32**, 117-124.
9. M. Fan, Y. Chen, Y. Xie, T. Yang, X. Shen, N. Xu, H. Yu and C. Yan, *Adv. Funct. Mater.*, 2016, **26**, 5019-5027.
10. Y. Cao, B. Zhang, X. Ou, Y. Li, C. Wang, L. Cao, C. Peng and J. Zhang, *New J. Chem.*, 2019, **43**, 7386-7392.
11. X.-W. Wang, H.-P. Guo, J. Liang, J.-F. Zhang, B. Zhang, J.-Z. Wang, W.-B. Luo, H.-K. Liu and S.-X. Dou, *Adv. Funct. Mater.*, 2018, **28**, 1801016.
12. Z. Li, L. Zhang, X. Ge, C. Li, S. Dong, C. Wang and L. Yin, *Nano Energy*, 2017, **32**, 494-502.
13. J. Li, L. Shi, J. Gao and G. Zhang, *Chem.-Euro. J.*, 2018, **24**, 1253-1258.
14. D. Zhao, R. Zhao, S. Dong, X. Miao, Z. Zhang, C. Wang and L. Yin, *Energy Environ. Sci.*, 2019, **12**, 2422-2432.
15. S. J. Clark, M. D. Segall, C. J. Pickard, P. J. Hasnip, M. J. Probert, K. Refson and M. C. Payne, *Z. Krist.-Cryst. Mater.*, 2005, **220**, 567-570.